Fundamentals of reservoir surface energy as related to surface properties, wettability, capillary action, and oil recovery from fractured reservoirs by spontaneous imbibition

DE-FC26-03NT15408

Quarterly Report
10/01/2004 – 12/31/2004

Norman R. Morrow, Principal Investigator
Herbert Fischer
Yu Li
Geoffrey Mason
Douglas Ruth
Siddhartha Seth
Peigui Yin
Shaochang Wo

February 2005

Submitted by:
Chemical & Petroleum Engineering
University of Wyoming
Dept. 3295, 1000 E. University Ave
Laramie, WY 82071

Disclaimer

ABSTRACT

The objective of this project is to increase oil recovery from fractured reservoirs through improved fundamental understanding of the process of spontaneous imbibition by which oil is displaced from the rock matrix into the fractures. Spontaneous imbibition is fundamentally dependent on the reservoir surface free energy but this has never been investigated for rocks. In this project, the surface free energy of rocks will be determined by using liquids that can be solidified within the rock pore space at selected saturations. Thin sections of the rock then provide a two-dimensional view of the rock minerals and the occupant phases. Saturations and oil/rock, water/rock, and oil/water surface areas will be determined by advanced petrographic analysis and the surface free energy which drives spontaneous imbibition will be determined as a function of increase in wetting phase saturation. The inherent loss in surface free energy resulting from capillary instabilities at the microscopic (pore level) scale will be distinguished from the decrease in surface free energy that drives spontaneous imbibition.

A mathematical network/numerical model will be developed and tested against experimental results of recovery versus time over broad variation of key factors such as rock properties, fluid phase viscosities, sample size, shape and boundary conditions. Two fundamentally important, but not previously considered, parameters of spontaneous imbibition, the capillary pressure acting to oppose production of oil at the outflow face and the pressure in the nonwetting phase at the no-flow boundary versus time, will also be measured and modeled. Simulation and network models will also be tested against special case solutions provided by analytic models.

In the second stage of the project, application of the fundamental concepts developed in the first stage of the project will be demonstrated. The fundamental ideas, measurements, and analytic/numerical modeling will be applied to mixed-wet rocks. Imbibition measurements will include novel sensitive pressure measurements designed to elucidate the basic mechanisms that determine induction time and drive the very slow rate of spontaneous imbibition commonly observed for mixed-wet rocks. In further demonstration of concepts, three approaches to improved oil recovery from fractured reservoirs will be tested; use of surfactants to promote imbibition in oil wet rocks by wettability alteration: manipulation of injection brine composition: reduction of the capillary back pressure which opposes production of oil at the fracture face.

TABLE OF CONTENTS

INTRODUCTION

Objectives

The long-range objective of this project is to improve oil recovery from fractured reservoirs through improved fundamental understanding of the process of spontaneous imbibition by which oil is displaced from the rock matrix into the fractures. Spontaneous imbibition is fundamentally dependent on the surface energy. An initial objective is to determine the surface energy and relate the dissipation of surface energy to the mechanism of spontaneous imbibition. A parallel objective is to model the mechanism of spontaneous imbibition by a combination of network analysis and numerical modeling. Also fundamentally important, but not previously considered, parameters of spontaneous imbibition, the capillary pressure acting to oppose production of oil at the outflow face and the pressure in the nonwetting phase at the no-flow boundary (in effect within oil in the non-invaded zone of the rock matrix) versus time, will also be measured and compared with values predicted by the mathematical model. The next objective is to measure surface energy and related spontaneous imbibition phenomena for mixed-wettability rocks prepared by adsorption from crude oil. The dissipation of surface free energy must then be related to oil production at mixed-wet conditions. The final objective is to apply the results of the project to improved oil recovery from fractured reservoirs in three ways: reduction of the capillary force that opposes oil production at the fracture face; change in wettability towards increased water wetness; identification of conditions where choice of invading brine composition can give improved recovery.

TASKS

Budget period 1, July 1, 2003 through June 30, 2005 – Ideas and Concept development: Fundamentals of Spontaneous Imbibition

Task 1. *Work of displacement and surface free energy.* Obtain complementary sets of capillary pressure drainage and imbibition data and data on changes in rock/brine, rock/oil, and oil/brine interfacial areas with change in saturation for drainage and imbibition for at least two rock types (sandstone and carbonate). Determine free-energy/work-of-displacement efficiency parameters for drainage and imbibition for at least two rock types so that changes in rock/wetting phase/nonwetting phase surface areas can be closely estimated from capillary pressure measurements.

Task 2. *Imbibition in simple laboratory and mathematical network models.* Study imbibition in at least three simple tube networks that can be modeled analytically to establish and/or confirm fundamental aspects of the pore scale mechanism of dynamic spontaneous imbibition with special emphasis on determining how spontaneous imbibition is initiated and the key factors in how the saturation profile develops with time. Incorporate rules developed from laboratory measurements on relatively simple networks into the design of a computational network model. Use the network model to obtain an account of the mechanism by which imbibition is initiated, the saturation profile is developed, and the rate of spontaneous imbibition in terms of the dissipation of surface free energy that accompanies change in saturation.

Task 3. *Novel observations on fluid pressures during imbibition and the mechanism of non-wetting phase production at the imbibition face.* Make novel observations on the imbibition mechanism including details of the mechanism of oil production at the outflow rock face and the change in the nonwetting phase pressure at the no-flow boundary of the core during the course of spontaneous imbibition for at least 16 distinct combinations of rock/ fluid properties.

Task 4. *Network/numerical model and new imbibition data.* Develop a numerical simulator specifically designed for spontaneous imbibition. Incorporate the network model to obtain a network/numerical model that includes matching the measured pressure in the nonwetting phase at the no-flow boundary, and the pressure that opposes production of oil at the open rock face. Imbibition data will be obtained for at least 10 rocks with over six-fold variation in permeability, and at least 6 orders of magnitude variation in viscosity ratio, and at least 10 variations in sample size, shape, and boundary conditions.

Task 5. *Comparison with similarity solutions.* Compare results given by simulation with special case analytic results given by similarity solutions for spontaneous imbibition for at least five distinct cases of rock and fluid properties.

Budget Period 2, July 1, 2005 through June 30, 2008 - Demonstration of concept: Application to mixed wettability rocks and improved oil recovery from fractures reservoirs.

Task 6. *Rock preparation and Work of displacement and surface areas*
Obtain a range of rock types and identify and obtain crude oils that induce stable mixed wettability. Prepare at least 25 rocks with mixed wettability through crude oil/brine/rock interactions.
Determine work of displacement for drainage and imbibition and measure the variation in rock/brine, rock oil, and oil/brine interfacial areas during the course of drainage and imbibition for at least two examples of mixed wettability.

Task 7. *Novel imbibition measurements on mixed-wet rock and network models.* Obtain, for at least six mixed-wet rocks, spontaneous imbibition data that includes measurements of the nonwetting phase pressure at the no-flow boundary, observations on the capillary pressure that resists production at the open rock face.

Task 8. *Application of network/numerical model to mixed wet rocks.* Use network models to relate dissipation of surface energy to rate of spontaneous imbibition and to account for the frequently observed induction time prior to the onset of spontaneous imbibition into mixed wettability rocks.

Task 9. *Increased oil recovery by spontaneous imbibition.* The mechanism of increased recovery from mixed wet rocks by use of surfactants that promote spontaneous imbibition by favorable wettability alteration will be investigated for at least four distinct examples of crude oil/brine/rock/surfactant combinations.
The mechanism of increased recovery by manipulation of brine composition will be investigated for at least four crude oil/brine/rock combinations.

Addition of very low concentration surfactants to the imbibing aqueous phase will be explored as a means of increasing the rate of oil recovery by reducing the capillary forces which resist production of oil at the fracture face. At least twelve combinations of rock and fluid properties including both very strongly wetted and mixed wet rocks will be tested.

PROGRESS BY TASK - BUDGET PERIOD 1

Task 1. *Work of displacement and surface free energy.*

Introduction

To obtain complementary sets of capillary pressure drainage and imbibition data and data on changes in rock/brine, rock/oil, and oil/brine interfacial areas with change in saturation for drainage and imbibition for at least two rock types (sandstone and carbonate). Determine free-energy/work-of-displacement efficiency parameters for drainage and imbibition for at least two rock types so that changes in rock/wetting phase/nonwetting phase surface areas can be closely estimated from capillary pressure measurements. This report provides an account of the petrophysical properties of Berea sandstone.

Experimental

SURFACE AREA AND PORE SIZE DISTRIBUTION ANALYSIS

BET[1] analysis

The total surface area of commonly occurring rocks, measured by nitrogen adsorption generally varies between 0.5 to 4 m^2/g for rocks even though permeability may vary over six orders of magnitude. In most sandstones, the majority of the contribution to the BET surface area comes from the clays that may include smectite, kaolinite, illite and, chlorite. The BET surface area of clay is about 15 m^2/g for kaolinite and chlorite, up to 800 m^2/g for smectite. Churcher et al. (1991) estimated the clay content of 6 to 8 % for an Upper Berea sandstone for which the variation in BET surface was 0.85 to 1.28 m^2/g. Based on the fact that the sample used in this study was a sandstone that had an BET surface area of 0.626 m^2/g, we expect the average clay content to be significantly less.

The different types of porosities i.e. micropores, mesopores and, macropores was studied for the sandstone used in this study, using both BJH and water adsorption/desorption analysis. The International Union of Pure Applied Chemistry (Everett, 1972) defined the different types of pores as follows:

Micropores: $r < 2$ nm
Mesopores: $r = 2 – 50$ nm
Macropores: $r > 50$ nm

BJH[4] analysis (mesopores)

A multi layer adsorption theory that included the effects of capillary condensation and multilayer adsorption was presented by Wheeler (1946). He suggested that effective radius of the pore was the sum of the multi-layer thickness from the BET theory. The pore size distribution was considered to have a Maxwellian or Gaussian distribution. Shull (1948) showed the inadequacy

of Wheeler's theory for the high pressure region and instead used a simple method of fitting data to a Maxwellian or Gaussian distribution function. Oulton (1948) proposed another method to get pore size distribution that did not assume any particular form of distribution but instead introduced another assumption that stated that the thickness of the adsorbed layer of the molecules on the pore wall is a constant. Barrett et al. (1951) showed that both the assumption of Maxwellian or Gaussian distribution function and the assumption of constant thickness for the adsorbed layer did not hold for some types of porous materials because of adsorption by capillary condensation. Kelvin's equation was used to calculate the capillary radii (sizes of pore) from the relative vapor pressure.

$$\log (P/P_0) = (-2*\sigma*V) / (8.316*10^7*2.303*T*r) \quad (1.1)$$

Where, σ is the surface tension of liquid nitrogen
V is the liquid molar volume of nitrogen
r is the radius of the capillary
T is the absolute temperature in ºK
$8.316 * 10^7$ is the gas constant in ergs/degree
P/P_0 is the relative humidity

For the BJH analysis, as explained by Barrett et al. (1951), incremental pore volumes of nitrogen adsorbed/desorbed are calculated at a given value of relative pressure. This volume is then converted to a value for capillary radii using Kelvin's equation (Eq 1.1). The exact procedure for determining capillary radii, r, is somewhat more complex than simple application of Eq 1.1. and will be discussed in a subsequent report. The area associated with the pore is calculated as:

$$A_p = 2 * V_p / r \quad (1.2)$$

The range of pore radii for which the data was collected in a BJH analysis extended from 1 – 74 nm. Hence most of the data corresponds to the mesopores. From the BJH analysis the surface area, hereby called BJH surface area, was 0.773 m^2/g for the sandstone sample.

Water adsorption desorption analysis (micropores, mesopores and, macropores)

Fischer et al. (2005) used water adsorption/desorption curves to characterize the porosity, ranging from micro to macroporosity, for a variety of rocks including the sandstone rock that was used in this study. The relative humidity, used for obtaining this data, was held constant at selected values by using glycerol/water mixtures of different proportions. Each specific value of relative humidity would then correspond to a value of pore radii that would fill at that value. The radii is calculated from Eq 1.3 and Eq 1.44 shown below

$$P/P_0 = \exp (-P_c* M) / (\rho RT) \quad (1.3)$$
$$r = 2 \sigma / P_c \quad (1.4)$$

Using the theory described for the BJH analysis, as described by Barrett et al. (1951) (Eq 1.2) an incremental area can be derived from the volume of water adsorbed for any given radii calculated from Eq 1.4. The data derived from a water adsorption/desorption isotherm is

shown in Fig 1. The cumulative increase in incremental area (for the same range of pore sizes as in the BJH analysis) could be compared to the value obtained by BJH analysis.

Results and Discussion

Summarizing the surface area obtained from three different analysis presented above we see that they fall in a fairly narrow range of 0.7 $\pm$ 0.1 m^2/g (BET 0.626 cm^2/g, BJH 0.773, water adsorption data 0.698 cm^2/g). Fig 1.1. includes the comparison between the incremental and cumulative areas as obtained from the water adsorption isotherm and the BJH analysis. The trend is similar for the two plots. One other important thing to note is that the BJH analysis was based on nitrogen adsorption rather than water.

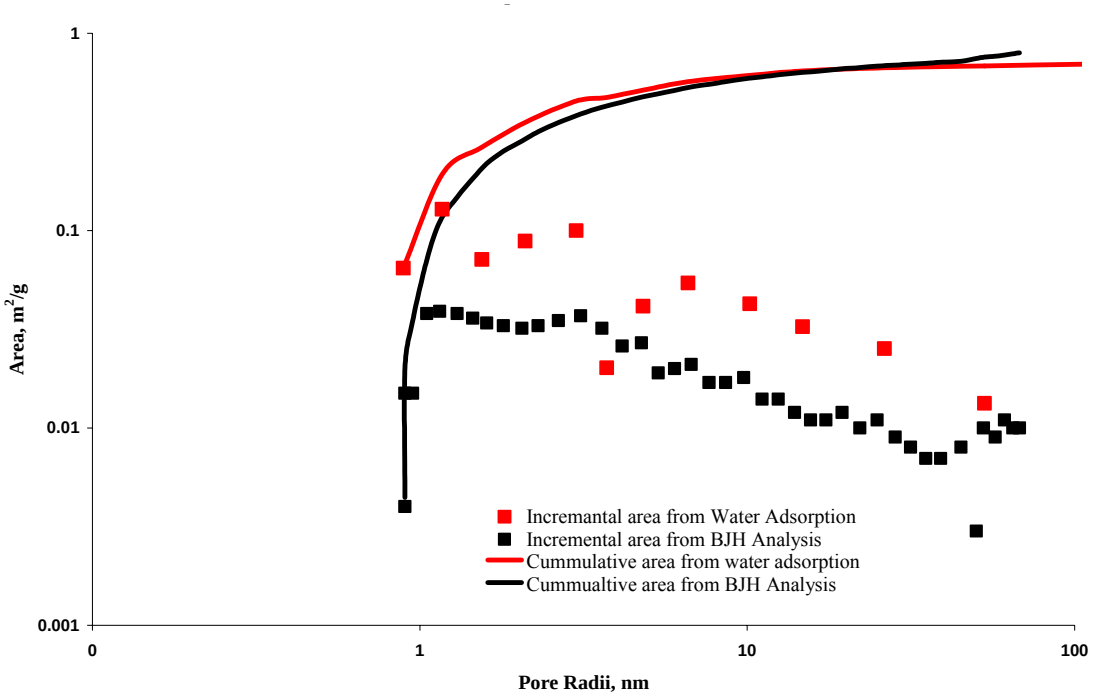

Fig. 1.1 Comparison of incremental area and cumulative area obtained from BJH analysis water adsorption isotherm

OTHER PETROPHYSICAL PROPERTIES

Permeability and porosity

The air permeability and the porosity of the sample was 740 md and 20% respectively.

SEM analysis

From the SEM pictures shown in Fig 1.2, 1.3, it is seen that the sandstone contained significant amounts of kaolinite and partially dissolved feldspar grains. The loosely packed kaolinite stacks fill intergranular spaces. Sheet like micropores exist between the pseudohexagonal plates. Micropores are also seen within the leached feldspar skeletons. Quartz overgrowth is developed between the detrital quartz grains, thus smoothing their originally rough surfaces.

XRD and clay analysis

The X-ray diffraction data for the sandstone sample is shown in Fig 1.4. Minor amounts of illite and chlorite are recognized from the XRD patterns, but these were very hard to identify from the SEM images. The clay analysis showed that the relative % of the kaolinite, illite and chlorite in the clays present in the sample is 66, 21 and, 13 respectively. The cation exchange capacity for the test sample was 0.00145 meq/g.

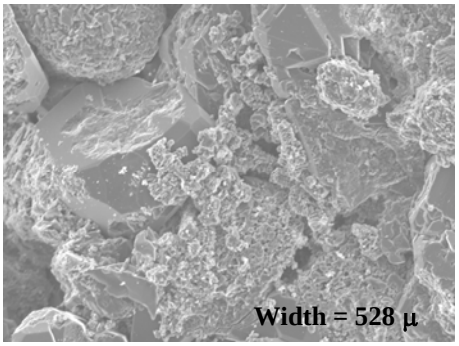

Fig 1.2 Kaolinite stacks filling the intergranular pores

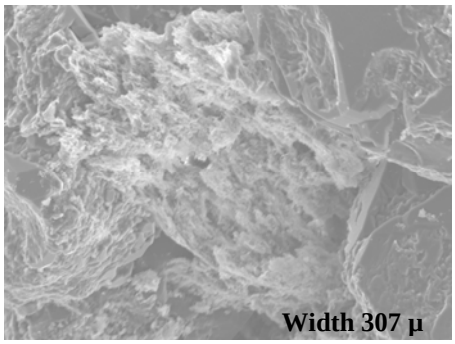

Fig 1.3 Partially dissolved feldspar grains

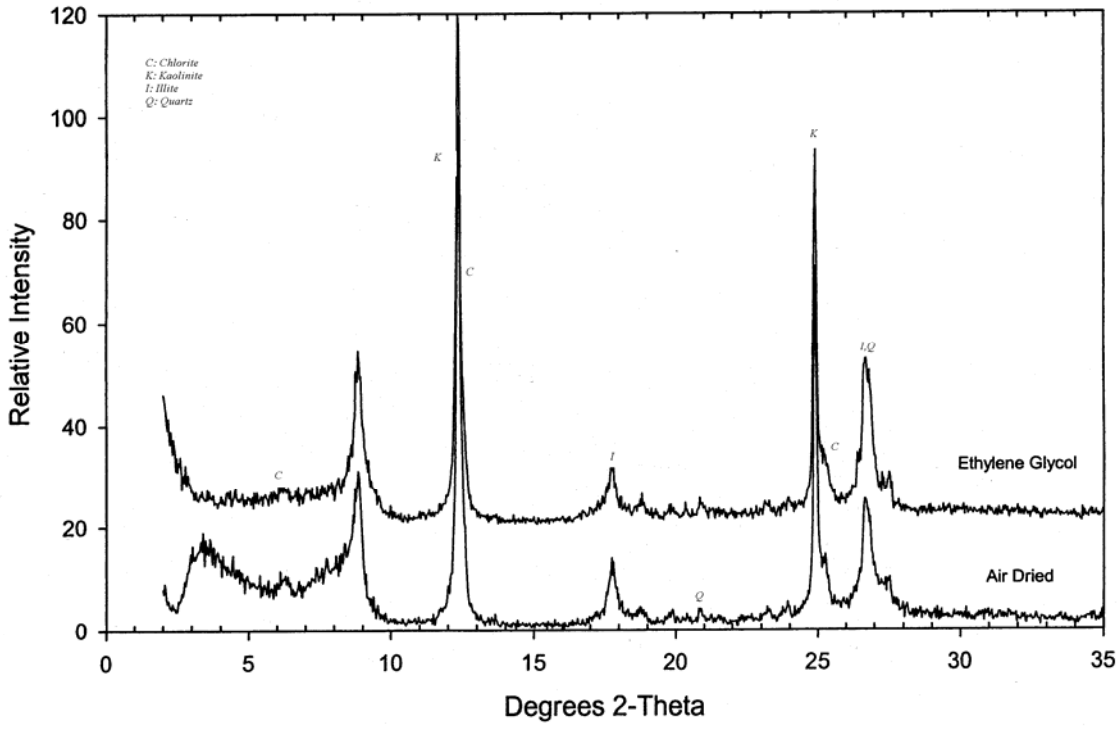

Fig 1.4 X-ray diffraction data for the sandstone sample

Task 2. *Imbibition in simple laboratory and mathematical network models.*

Introduction

The effect of pore geometry and wetting on capillary displacement pressure has been studied theoretically for a wide variety of pore shapes, using developments of the theory of Mayer and Stowe and Princen, and experimentally for a wide variety of shapes of pore formed from assemblies of rods, plates and spheres (for example, Mason et al., 1983; Mason and Morrow, 1986, 1987, 1991; Ma et al., 1996). Network models of pores have also been studied extensively for example Mason (1971), Sorbie (Dixit et al., 1999), Blunt (1997), and Oren (Oren et al., 1998) but development of network models for spontaneous imbibition lag well behind other advances. One indication of need for a network model is provided by preliminary observations of imbibition by a one end open core. Pressure build up in the nonwetting phase, monitored via a pressure tap, showed a distinct time lag. Such observations indicate that the longstanding assumption (Blair, 1964; Pooladi-Darvish and Firoozabadi, 2000) that capillary pressure immediately rises to a set value, corresponding to residual nonwetting phase saturation at the open core face, needs to be reconsidered. Both this pressure build up and the capillary back-pressure that opposes production of the nonwetting phase at the outflow face must be accounted for in a fundamentally sound network model of counter-current imbibition.

The pressure build up in the non-wetting phase, as observed for imbibition by a one end open core, is closely related to the capillary back-pressure that opposes production of the non-wetting phase at the outflow face. At the pore scale, the complexity of the boundary conditions at the interfaces between fluids and between the fluids and the solid rock matrix means that an exact mathematical description is often difficult to obtain for all but the simplest cases. Moreover, the fluid motion at the three-phase contact line between moving immiscible fluids and a solid boundary is still not completely understood. Nevertheless it is possible to predict the fluid flow in several idealized pore geometries, such as through cylindrical tubes. In spontaneous imbibition, capillary pressure is considered as the dominant driving force, and Poiseuille's law covers practically the whole range of flow rate.

In the preceding quarterly report, we presented a simple network model that consists of a number of pore cell units, described as "Hub-and-Spoke Units". Each Unit consists of a sphere (hub) and several connecting cylindrical tubes (spokes) as illustrated in Figure 2.1. Each tube of a Hub-and-Spoke Unit can be classified by one of three possible cases: tube end is open to the network boundary; end is a closed end; or end is connected (shared) with another Hub-and-Spoke Unit. Based on Poiseuille's law, mathematical models have been derived for spontaneous imbibition of water against gas and water against oil in the Hub-and-Spoke Units. Even for a unit cell, it is difficult to find general analytical solutions, except for some simple configurations. Numerical solving schemes and computer codes have, therefore, been developed to simulate the imbibition process in the Hub-and-Spoke Units. In this quarterly report, details of a numerical solving procedure are presented for spontaneous imbibition of water against gas along with some simulation results. Numerical simulation of spontaneous imbibition of water against oil is currently in progress.

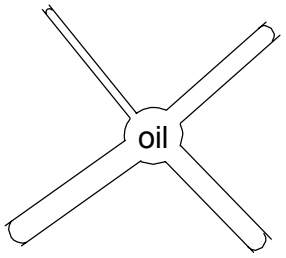

Figure 2.1. A Hub and Spoke Unit with four open-ended tubes.

Experimental

Spontaneous imbibition of water against oil in Hub-and-Spoke Units

When gravitational effects are negligible, capillary pressure becomes the dominant driving force in spontaneous imbibition. As presented in the preceding quarterly report, the spontaneous imbibition of water replacing oil in a Hub-and-Spoke Unit can be described by Poiseuille's law (Eqs. 2.1 and 2.2), the flow differential equation of Eq. 2.3, and the volume balance equation of Eq. 2.4, in which water and oil are considered as incompressible fluids.

$$q_{iw}^* = \frac{\pi(p_{out}^* - p_{iw}^*)(r_i^*)^4}{x_i^*} b \qquad (2.1)$$

$$q_{io}^* = \frac{\pi(p_{io}^* - p^*(t))(r_i^*)^4}{L_i^* - x_i^*} (\frac{\mu_w}{\mu_o}) b \qquad (2.2)$$

$$i = 1,2,\cdots n$$

$$\pi(r_i^*)^2 dx_i^* = q_{iw}^* \frac{dt_D}{b} \quad \text{and} \quad q_{io}^* = q_{iw}^* \qquad (2.3)$$

$$i = 1,2,\cdots n$$

$$\sum_i q_{io}^* = 0 \qquad (2.4)$$

For generality, we assume that the Unit has *n* tubes of radii $r_1 \le r_2 \le \cdots \le r_n$. All tubes are open to the network boundary and the hub has no volume in the following simulated cases. In Eqs. 2.1 to 2.4, parameters *a* and *b* are defined as:

$$a = \frac{2\sigma\cos\theta}{PL}, \quad b = \frac{P}{8\mu_w} \qquad (2.5)$$

Dimensionless time is defined by

$$t_D = bt \qquad (2.6)$$

The dimensionless radius, length, and invading position are defined by

$$r_i^* = \frac{r_i}{L}, L_i^* = \frac{L_i}{L}, x_i^* = \frac{x_i}{L}, i = 1 \sim n \tag{2.7}$$

The dimensionless pressure at the center of the Hub-and-Spoke Unit, $p^*(t)$, and the dimensionless bulk water pressure outside the Unit, p_{out}^*, are defined by

$$p^*(t) = \frac{p(t)}{P}, \; p_{out}^* = \frac{p_{out}}{P} \tag{2.8}$$

Where *P* is the unit of pressure measurement; *p(t)* is the pressure inside the sphere of the Hub-and-Spoke Unit at any given time *t*. Similarly, the dimensionless capillary pressure in tube *i* is defined by

$$p_{ci}^* = \frac{p_{ci}}{P} = \frac{a}{r_i^*} = p_{io}^* - p_{iw}^* \tag{2.9}$$

In Eq. 2.10, the redefined water and oil flow rates are not dimensionless but have units of *1/t*. However, the time unit can be eliminated from the flow differential equation of Eq. 2.3.

$$q_{iw}^* = \frac{q_{iw}}{L^3}, q_{io}^* = \frac{q_{io}}{L^3} \tag{2.10}$$

Where *L* is the unit of length measurement; $L_1, L_2, \cdots, L_n$ are the tube lengths; and $x_1, x_2, \cdots, x_n$ are the invading water front positions in tubes at any given time *t*.

For most cases, it will not be easy to find an analytical solution for Eqs. 2.1 to 2.4 but they can be solved numerically. A numerical scheme and its computer code have been developed to simulate water imbibing against oil in a Hub-and-Spoke Unit. The simulation procedure is described in below.

Assuming that we have obtained the advancing/retreating positions of the menisci in tubes, $x_i^{*t_D}, i = 1 \sim n$, at time t_D, for a given time increment Δt_D, we want to calculate the updated meniscus positions, $x_i^{*t_D+\Delta t_D}, i = 1 \sim n$. The computation can be summarized by three steps:

(1) Knowing $x_i^{*t_D}$, $p_{iw}^*(t_D), p_{io}^*(t_D), p^*(t_D), i = 1 \sim n$

(2) Calculating $x_i^{*t_D+\Delta t_D}, i = 1 \sim n$ from Eq. 2.3

(3) Updating the Hub pressure, $p^*(t_D + \Delta t_D)$, by

$$p^*(t_D + \Delta t_D) = \sum_i \frac{(p_{out}^* + \frac{a}{r_i^*})(r_i^*)^4}{L_i^* + x_i^{*t_D+\Delta t_D}(\frac{\mu_w}{\mu_o} - 1)} \Big/ \sum_i \frac{(r_i^*)^4}{L_i^* + x_i^{*t_D+\Delta t_D}(\frac{\mu_w}{\mu_o} - 1)} \tag{2.11}$$

(4) Updating the oil phase pressures at menisci, $p_{io}^*(t_D + \Delta t_D), i = 1 \sim n,$ by

$$p_{io}^{*}(t_D+\Delta t_D)=\frac{x_i^{*t_D+\Delta t_D}\dfrac{\mu_w}{\mu_o}}{L_i^{*}+x_i^{*t_D+\Delta t_D}(\dfrac{\mu_w}{\mu_o}-1)}p^{*}(t_D+\Delta t_D)+\frac{L_i^{*}-x_i^{*t_D+\Delta t_D}}{L_i^{*}+x_i^{*t_D+\Delta t_D}(\dfrac{\mu_w}{\mu_o}-1)}(p_{out}^{*}+\frac{a}{r_i^{*}}) \tag{2.12}$$

(5) Updating the water phase pressures at menisci, $p_{iw}^{*}(t_D+\Delta t_D), i=1\sim n,$ from Eq. 2.9

The above five steps for each time increment are repeated until the spontaneous imbibition process is completed. At the end of imbibition, oil is trapped only in the tubes with the largest radii in the Unit.

Spontaneous imbibition of water replacing gas in Hub-and-Spoke Units

The same configuration of Hub-and-Spoke Unit was used to simulate the spontaneous imbibition of water against gas. Here, the Unit is initially saturated with gas instead of oil and the gas viscosity is negligible. The numerical solving scheme for water-gas spontaneous imbibition was initially introduced in the last quarterly report. For consistency, derivation of the mathematical model derivation and its numerical solving scheme are presented.

When the gas inside the Unit is compressed by invading water, the gas can be assumed to obey Boyle's Law: for a given mass, at constant temperature, the pressure times the volume is a constant.

$$pV = mRT \tag{2.13}$$

where p is the gas pressure, V is the gas volume, T is temperature, m is the number of moles, and R is the gas constant. For air, R=0.286 kJ/kg/^{o}K.

Let V^0 and V^t represent the initial gas volume and the gas volume at time t. We have

$$V^0=\sum_i \pi L_i r_i^2, \quad V^t=\sum_i \pi(L_i-x_i^t)r_i^2 \tag{2.14}$$

or in the dimensionless format

$$V^{*0}=\frac{V^0}{L^3}=\sum_i \pi L_i^{*} r_i^{*2}, \quad V^{*t}=\frac{V^t}{L^3}=\sum_i \pi(L_i^{*}-x_i^{*t})r_i^{*2} \tag{2.15}$$
$$i=1,2,\cdots n$$

According to Boyle's Law of Eq. 2.22, we obtain

$$p^{*}(t_D)=\frac{p^{*0}V^{*0}}{V^{*t_D}} \tag{2.16}$$

In addition, if the gas viscosity is neglected, gas pressure is the same everywhere inside the Hub and Spoke Unit. For the trapped gas, Poiseuille's law (Eq. 2.1) gives,

$$q_{iw}^{*} = \frac{\pi(p_{out}^{*} - (p^{*}(t_D) - p_{ci}^{*}))r_i^{*4}}{8\mu_w x_i^t} b \qquad (2.17)$$
$$i = 1,2,\cdots n$$

Eqs. 2.3, 2.15, 2.16, and 2.17 form the mathematical model for the water-gas spontaneous imbibition in a Hub-and-Spoke Unit. A numerical scheme, described below, has been developed to solve the proposed mathematical model.

Assuming that we have obtained the advancing/retreating positions in each tube, $x_i^{*t_D}, i = 1 \sim n$, at time $t_{D,}$ for a given time increment Δt_D, we want to calculate $x_i^{*t_D+\Delta t_D}, i = 1 \sim n$. The computation can be summarized by three steps:

(1) Knowing $x_i^{*t_D}$, $p^{*}(t_D), i = 1 \sim n$

(2) Calculating $x_i^{*t_D+\Delta t_D}, i = 1 \sim n$ from Eqs. 2.3 and 2.17, precisely,

If $(p_{out}^{*} - (p^{*}(t_D) - p_{ci}^{*})) \geq 0$ then $x_i^{*t_D+\Delta t_D} = \sqrt{(x_i^{*t_D})^2 + 2(p_{out}^{*} - p^{*}(t_D) + p_{ci}^{*})(r_i^{*})^2 \Delta t_D}$

If $(p_{out}^{*} - (p^{*}(t_D) - p_{ci}^{*})) < 0$ then $x_i^{*t_D+\Delta t_D} = 2x_i^{*t_D} - \sqrt{(x_i^{*t_D})^2 - 2(p_{out}^{*} - p^{*}(t_D) + p_{ci}^{*})(r_i^{*})^2 \Delta t_D}$

(3) Updating $p^{*}(t_D)$ from Eqs. 2.15 and 2.16.

The above three steps are repeated for each time increment until the spontaneous imbibition process is complete. When imbibition begins, water invades every tube so gas inside the unit is compressed. Once the compression phase is finished, the gas bubble inside the Unit will expand and be pushed out from the largest tube(s), by the capillary pressure acting in the smaller tubes. At the end of imbibition, gas is trapped only in the largest tube(s) of the Unit. Some of the simulation results are presented in the next section.

Results and Discussion

Coded by C++, console applications have been developed for simulating the spontaneous imbibition in the Hub-and-Spoke Units. The two codes, named SpiderWO and SpiderGas, are used to simulate the imbibitions of water against oil and gas, respectively. Examples of the formatted input files for SpiderWO and SpiderGas are shown in Figure 2.2 and 2.3. For a simulation run, the input file defines the configuration of a Hub-and-Spoke Unit, initial pressures, total simulation time, time step and printing time step. With various parameter settings, the time-lag phenomena at different pore scales can be investigated by the simulation. Some preliminary results are discussed below.

```
//This is a formatted input file for SpiderWO (water/oil). Please do not insert or delete any lines.
//Dimensionless Units are used in computation
//Using a space to separate parameters if they are entered in one line.
## Begin of data input: unit length - cm, time - second
//--- Initial outside (water) pressure (in psi) & the scale-pressure (in dynes/cm2)
14.7 1.0
//--- a & b (two parameters), Lambda: water/oil viscosity ratio ---
60.0 12.5 1.5
//--- TD & delta tD, print_step (i.e. printing once for every print_step of tD) ---
100 0.002 10
//--- Tube Configuration ---
//Number of tubes
5
//--- Tube Length ---
1 1 1 1 1
//--- Tube Radius ---
0.005 0.007 0.008 0.009 0.01
## End of data input
```

Figure 2.2. Example of the formatted input file for the SpiderWO console application.

```
//This is a formatted input file for SpiderGas. Please do not insert or delete any lines.
//Dimensionless Units are used in computation
//Using a space to separate parameters if they are entered in one line.
## Begin of data input: unit length - cm, time - second
//--- Initial outside (water) pressure and inside (gas) Pressure (in psi) & the scale-pressure (in dynes/cm2)
14.7 14.7 1.0
//--- a & b (two parameters) --- contact angle = 0 degree
140.0 12.5
//--- TD & delta tD, print_step (i.e. printing once for every print_step of tD) ---
0.002 0.00002 1
//--- Tube Configuration ---
//Number of tubes
5
//--- Tube Length ---
1 1 1 1 1
//--- Tube Radius ---
0.005 0.007 0.008 0.009 0.01
## End of data input
```

Figure 2.3. Example of the formatted input file for the SpiderGas console application.

Imbibition simulation of water against gas

As observed in laboratory experiments on core samples, the gas in core samples is first compressed at the beginning of a spontaneous imbibition process until gas breaks through from the pores with the largest size in diameter at the outflow face. When the gas inside the Unit is compressed by invading water, the gas obeys the Boyle's Law and, therefore, an increase in gas pressure is observed. In this first attempt, a single Hub-and-Spoke Unit was used to simulate the, so called, time-lag that precedes gas production. The configuration of the Unit is given in Table 2.1. The fluid properties, initial condition, and other parameter settings used in the simulation are listed in Table 2.2. The wettability effect was simulated by using different contact angles.

Table 2.1. The configuration of the simulated Hub-and-Spoke unit

Hub Volume	0	
Spoke	**Radius, μm**	**Length, cm**
Spoke 1	50	1
Spoke 2	70	1
Spoke 3	80	1
Spoke 4	90	1
Spoke 5	100	1

Table 2.2. Fluid properties and parameters used in water replacing gas

Initial gas pressure inside the Unit, psi	14.7
Bulk water pressure outside the Unit, psi	14.7
Water viscosity, μ_w, cp	1
Water-gas interfacial tension, σ, dyn/cm	70
Contact angle, degree	0, 15, 30, 45
a	140, 135, 121, 99
b, 1/second	12.5

Note that, in Table 2.1, the hub volume was assumed to be in the simulations. The assumption was used, as a demonstration, for simplifying the computation only. In a network model that represents a certain porous medium, the total volume of the Hubs and Spokes in a cubic unit can be set equal to the porosity of the given porous medium.

As shown in Figs. 2.4 and 2.5, the contact angle, through its effect as a boundary condition on capillary pressure, has a notable effect on the initial gas compression and the gas recovery rate. For a larger contact angle and the associated reduced capillary pressures, it takes less time for compression of the gas, Fig. 2.4, but more time for recovering the gas from the Unit, Fig. 2.5. During the compression phase, water-gas menisci in all tubes first move towards the Hub as the gas pressure builds up, Figs. 2.4 and 2.6. After reaching a pressure equilibrium, the gas bubble inside the Unit begins to move toward the largest tube of the Unit, Fig. 2.6. As the gas bubble expands again its pressure drops accordingly, Fig. 2.4, before gas breakthrough from the Unit. Figure 2.7 shows the dimensionless water flow rate in each spoke before gas breakthrough. The dimensionless flow rate is defined by Eq. 2.18, where q^* is the flow rate given by Eq. 2.10 or 2.17.

$$q_D = q^* / b \tag{2.18}$$

As shown in Fig. 2.7, the water outflow rate in the tube of 100 μm radius increases rapidly when its water-gas meniscus approaches the tube's outlet end. Because the gas viscosity is neglected and therefore the gas pressure is the same everywhere in the Unit, the gas bubble can only flow out through tubes with the largest radius. This flow pattern will not always be true for imbibition of water against oil, as will be demonstrated in the next quarterly report.

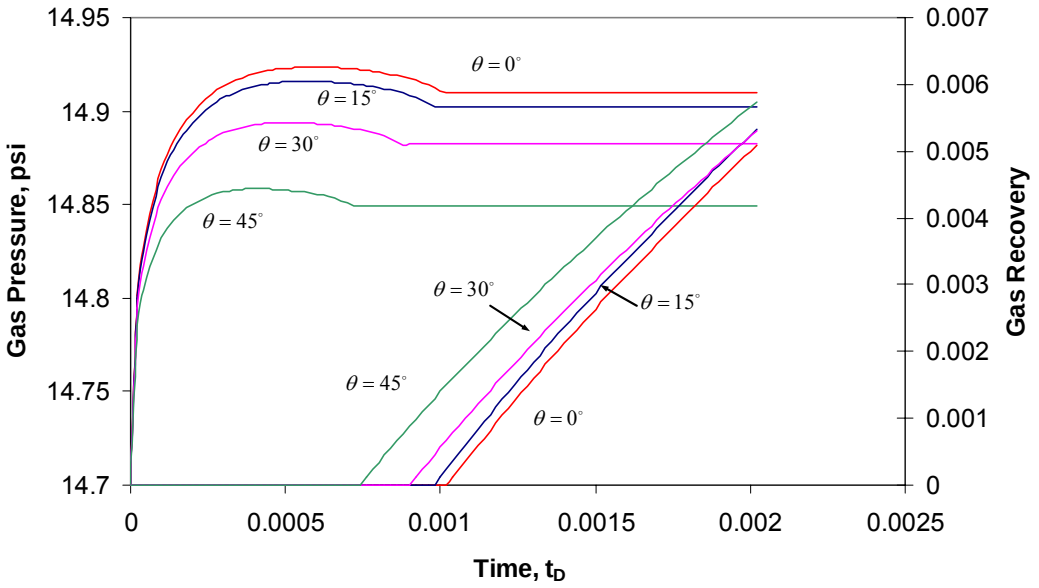

Figure 2.4. The effect of contact angle on the initial gas compression and the recovery induction time.

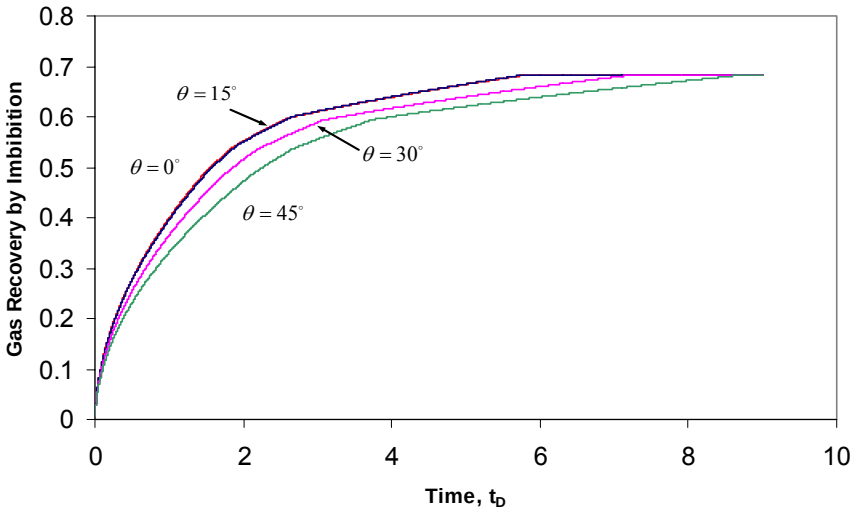

Figure 2.5. The gas recovery rates simulated by using different contact angles

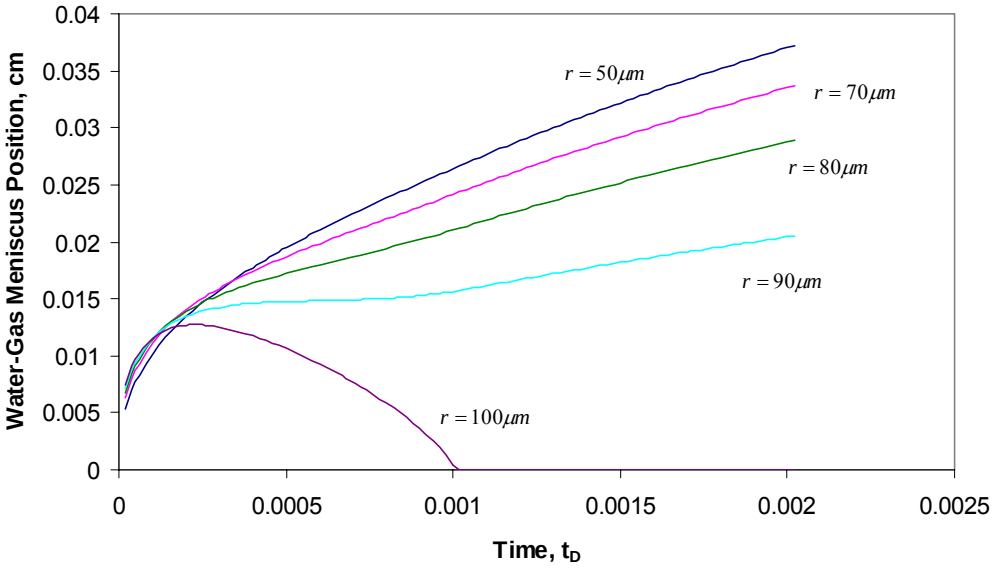

Figure 2.6. The advancing/receding behavior of water-gas menisci in spokes during the initial gas compression phase of spontaneous imbibition (contact angle = 0°).

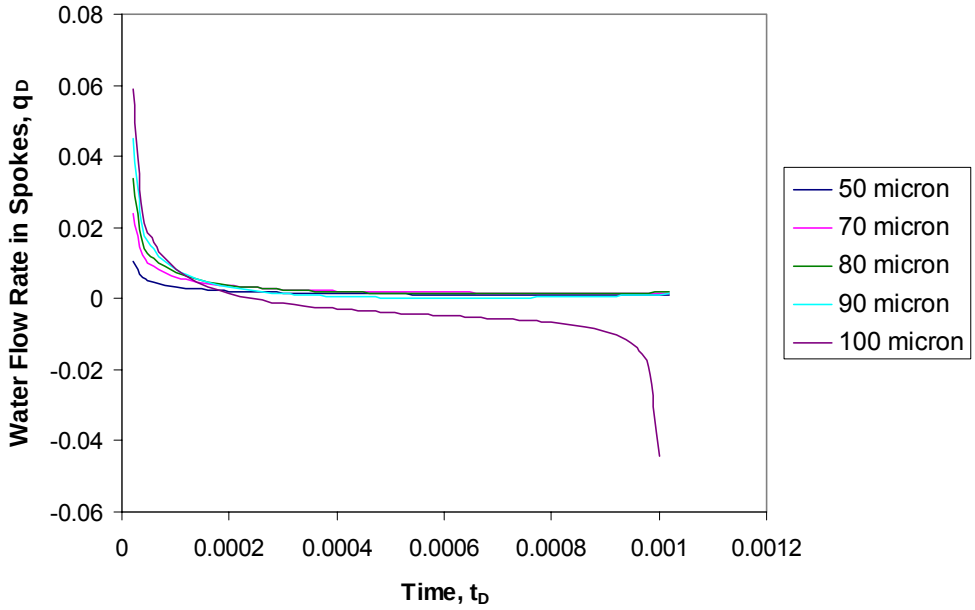

Figure 2.7. The water flow rates in spokes before gas breakthrough from the spoke with the largest radius (contact angle = 0°).

Task 3. *Novel observations on fluid pressures during imbibition and the mechanism of non-wetting phase production at the imbibition face.*

Introduction

The mathematical model used to develop previously reported simulations is presented below together with the functions used to describe variation in capillary pressure and relative permeabilities.

Mathematical model

The basic equations used for deducing the similarity solutions have been given in the simulation method described in Ruth et al [2000].

$$\frac{\partial}{\partial x}\left[\bar{\lambda}\frac{\partial P_c}{\partial x}\right] = \phi\frac{\partial S_w}{\partial t} \tag{3.1}$$

where average mobility, $\bar{\lambda}$ is a function of saturation only and is defined as

$$\bar{\lambda} = \frac{Kk_{rw}k_{rnw}}{\mu_w k_{rnw} + \mu_{nw}k_{rw}} \tag{3.2}$$

Note that this equation is not a pair of simultaneous parabolic partial differential equations in unknown pressure in the WP and NW as is usually obtained. Instead it is only one parabolic partial differential equation in known capillary pressure, P_c. A finite difference equation can be derived immediately (Eq. 3.1).

$$\Delta S_{w(i)} = \frac{1}{V_\phi}[Tr_{(i-1+1/2)}(P_{c(i)} - P_{c(i-1)}) - Tr_{(i+1/2)}(P_{c(i+1)} - P_{c(i)})]\Delta t \tag{3.3}$$

where i is the ordinal number of the grids, and $Tr_{(i+1/2)} = \frac{A}{2\Delta x}(\bar{\lambda}_{(i)} + \bar{\lambda}_{(i+1)})$ is the mean transmissibility from midpoint weighing. This approximation is of second-order, which helps to produce fast convergence of results (Fig. 3.1). The more common upsteam weighting is a first-order approximation. Using this weighting, no convergence could be obtained for the water/oil case. Even using a fast personal computer, a single simulation was not found even after many days. Why upsteam weighting can not produce results in some COUCSI simulations in a timely manner needs to be further explored.

The starting condition for COUCSI is

$$S_w = S_{wi} \tag{3.4}$$

for the partial differential equation (Eq. 3.1), where S_{wi} is the original WP saturation.
in the finite difference equation (Eq. 3.3)

$$S_{w(i)} = S_{wi(i)} \tag{3.5}$$

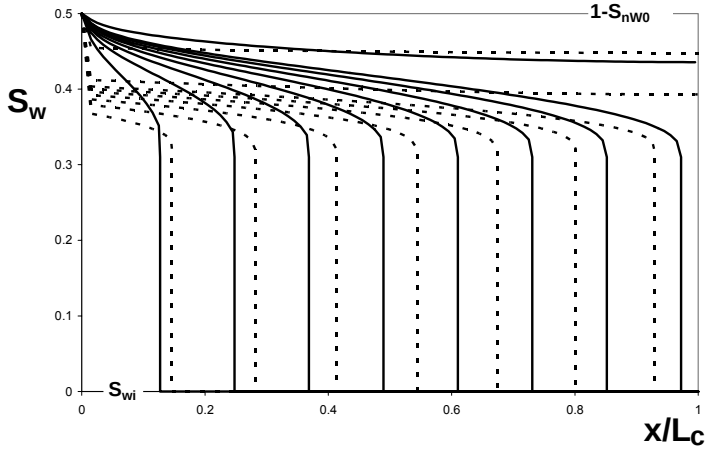

Fig. 3.1 Comparison of the profiles calculated from the programs based on midpoint weighting (solid lines) and upsteam weighting (broken lines) The results were generated for Δx=100, Δt=0.05. The intervals of recovery, Q_w/V_ϕ, are 0.05.

Experimental

With the boundary condition for the general COUCSI partial differential equation (Eq. 3.1) as:

$$P_w = 0 \quad at \quad x = 0 \tag{3.6}$$

Also

$$q_w = q_{nw} = 0 \quad at \quad x = L_C \tag{3.7}$$

If the number of total grids for the core is *N-2* and if Grid *1* is for the *WP* reservoir and Grid *N* is for the grid with a mirror image of the last core grid, Grid *N-1*, the corresponding boundary condition for the above general finite difference equation can be written as

$$S_{w(1)} = S_{w0} \quad at \quad i = 1 \tag{3.8}$$

and

$$S_{w(n)} = S_{w\ (n-1)} \quad at \quad i = N \tag{3.9}$$

where S_{nw0} is the final recovery for COUCSI in the simulation.

Since every parameter or variable is known, the finite difference equation (Eq. 3.3) is an explicit function, by which the saturation increment for each grid can be calculated for each time step. The numerical simulation will produce a saturation profile varying with time. q_w, q_{nw}, P_w and P_{nw} need not be calculated directly in the simulation. They can be readily obtained from the saturation profiles in the output file.

Results and Discussion

To obtain the saturation profile without distortion ('in conditional stability' as described in Aziz, (1979) the time step, Δt, must be less than a limit for a certain division x/L_c. From this study, if x/L_c is fixed and Δt is under the time step limit, the resultant profile will be the same no matter what Δt is used. As is already known (Richtmyer and Morton, 1967), there exists a constant $(x/L_c)\Delta t$, the upper limit for which is the so called 'condition of stability' in the simulation of a given Buckley-Leverett flow. However for our program, it was found that there existed a constant $(x/L_c)^2\Delta t$ for the upper limit (Fig. 3.2) in COUCSI. Therefore, to obtain a COUCSI result with a high degree of convergence, much more calculation time is required.

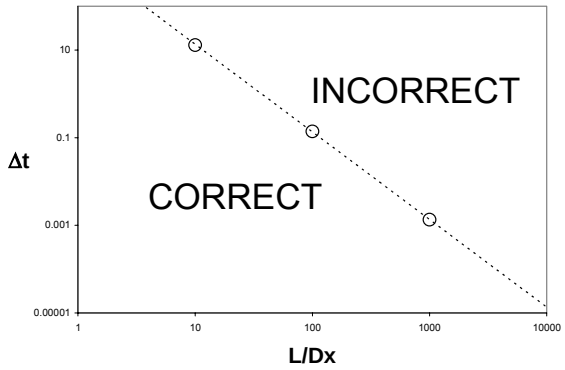

Fig. 3.2 Condition for the results without distortion in H8O simulation. Points represent the tested critical points. The broken line represents the division between 'correct' and 'incorrect' results for any chosen grid. Correct results do not depend on the size of the time step. 'Incorrect' results vary with the size of the time step.

Task 4. *Network/numerical model and new imbibition data.*

Introduction

New imbibition data with non-matched liquid viscosities and the all faces open boundary condition (NM(4), NM(22) and NM(43)) were presented in previous quarterly reports. In this report new imbibition data at very strongly water-wet conditions are presented that were obtained with matched liquid viscosities (with viscosity ratios close to unity) and the all faces open boundary condition. Matched viscosities ranged from 4 to 172 cp. The imbibition curves were closely correlated over the entire viscosity range. Overall, an increase of the matched viscosity was accompanied by only a slight increase of the final oil recovery. All of the oil recovery curves exhibited essentially the same shape.

Experimental

MATERIALS

The same liquids and sandstone cores as utilized in the sets with non-matched viscosities (NM(4), NM(22), NM(43)) were used for all tests in this experimental set. The preparation steps were also identical to the aforementioned experimental sets.

As for the data sets with non-matched liquid viscosities, the all faces open boundary condition entails 3-dimensional fluid flow. The characteristic length, L_c, for each core is then defined by (Zhang et al., 1996)

$$L_c = \frac{ld}{2\sqrt{d^2 + 2l^2}} \tag{4.1}$$

and was close to 1.24 cm for each core as a result of the identical size and geometry. Oil production as a function of time was measured in standard imbibition cells at ambient temperature and with 0% initial water saturation for each test.

Results and Discussion

Imbibition results for matched viscosity were correlated by the scaling group proposed by Mattax and Kyte,

$$t_{D,MK} = t\sqrt{\frac{k}{\phi}}\frac{\sigma}{\mu_w}\frac{1}{L^2} \tag{4.2}$$

SPONTANEOUS IMBIBITION

The scaling equation of Mattax and Kyte was proposed for the special case of matched viscosities. In the present work the equation was tested for a constant viscosity ratio very close to unity for a wide range of matched viscosities. The viscosity ratio, Ψ, is defined by

$$\Psi = \mu_{ap} / \mu_o \tag{4.3}$$

Table 4.1 lists the core and liquid properties used for this experimental set.

Table 4.1 Rock and Fluid Properties, Matched Viscosities									
Core #	L_c cm	k_g md	Φ %	σ_{ow} dyn/cm	ρ_{ap} g/cm^3	ρ_o g/cm^3	μ_{ap} cP	μ_o cP	μ_g cP
C1-20	1.239	71.2	17.4	40.2	1.119	0.782	4.3	4.0	4.1
C1-24	1.240	59.7	17.4	36.8	1.170	0.817	13.6	13.6	13.6
C1-21	1.238	72.2	17.5	34.4	1.185	0.828	20.9	20.9	20.9
C1-19	1.237	69.9	17.5	33.3	1.204	0.843	43.9	44.1	44.0
C1-23	1.244	66.5	17.7	32.0	1.213	0.851	59.3	59.3	59.2
C1-22	1.236	69.7	17.9	31.8	1.220	0.858	80.2	80.1	80.1
C3-30	1.238	63.1	17.1	30.5	1.226	0.863	99.7	99.1	99.4
C5-4	1.230	69.6	17.4	30.1	1.231	0.869	140.0	141.7	140.8
C3-34	1.242	75.8	17.7	30.3	1.235	0.873	171.2	173.0	172.1

Relationships between oil recovery and imbibition time are presented in Fig. 4.1. The rate of oil recovery systematically decreases as viscosity increases (Fig. 4.1a). A close correlation of results over the entire viscosity range was obtained with the Mattax and Kyte scaling group (Fig. 4.1b). The shapes of the correlated oil recovery curves were all the same and no distinct trend with respect to absolute values of viscosity was recognizable. A slight overall increase of final oil recovery with viscosity ratio was observed (Fig. 4.1c), however, all data points but one fell within 52 % ± 1.

Fig. 4.2a shows the dependency of the imbibition time for percent of normalized final recovery ranging from 20 to 98 % for the nine matched viscosity experiments. The curves are characterized by a close to parallel alignment with increase in recovery. Close correlation of the imbibition results is further demonstrated by Fig. 4.2b, which displays the dimensionless times for a specific recovery as a function of matched viscosity. The curves fall close to horizontal straight lines that correspond to perfect correlation.

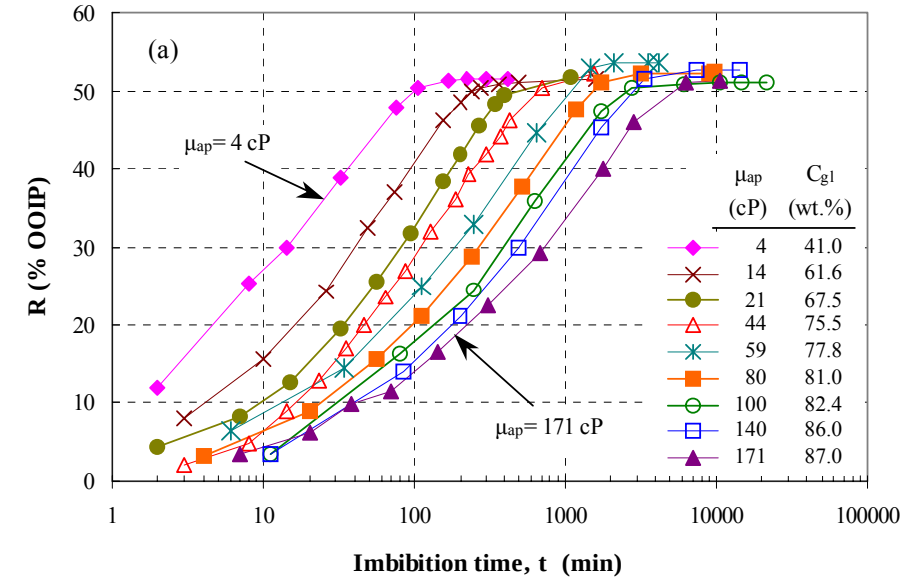

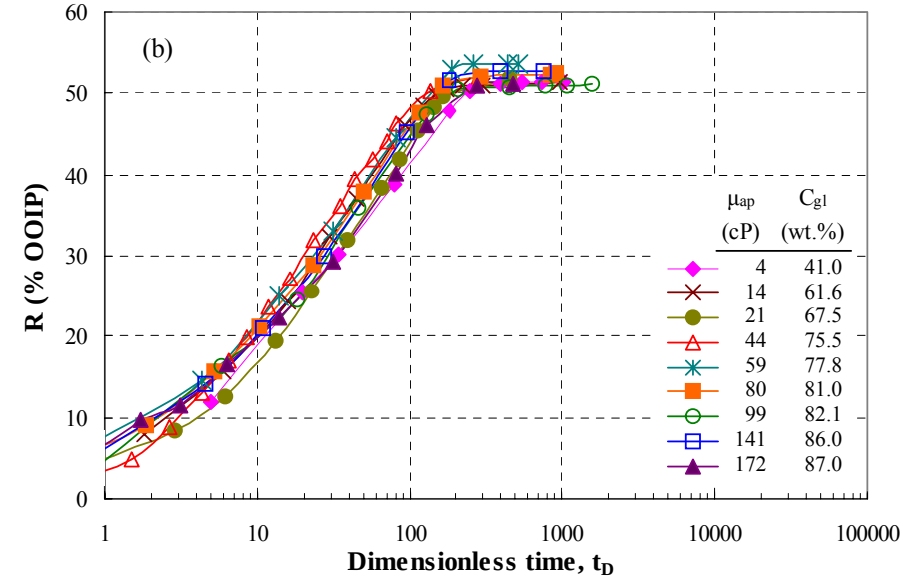

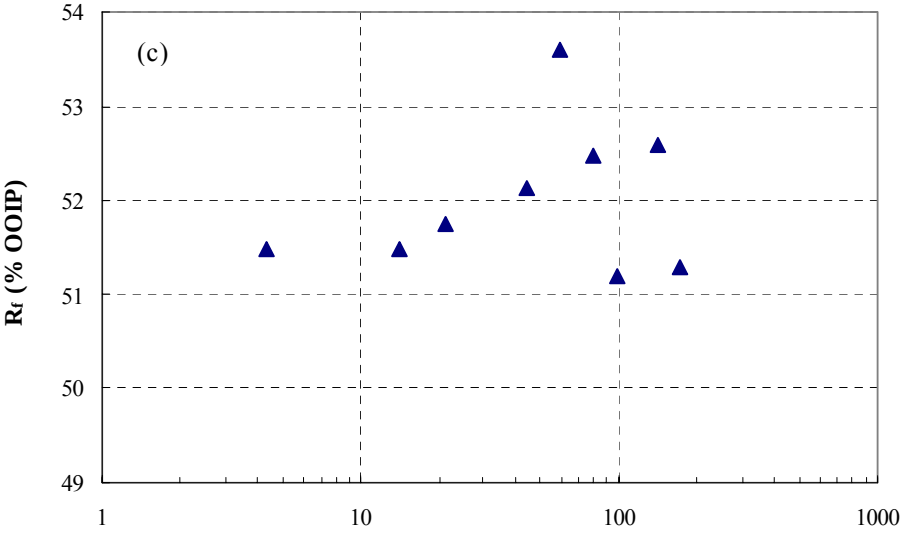

Fig. 4.1 Recovery of oil by spontaneous imbibition for matched phase viscosity versus (a) time and (b) dimensionless time; (c) final oil recovery, R_f, versus viscosity.

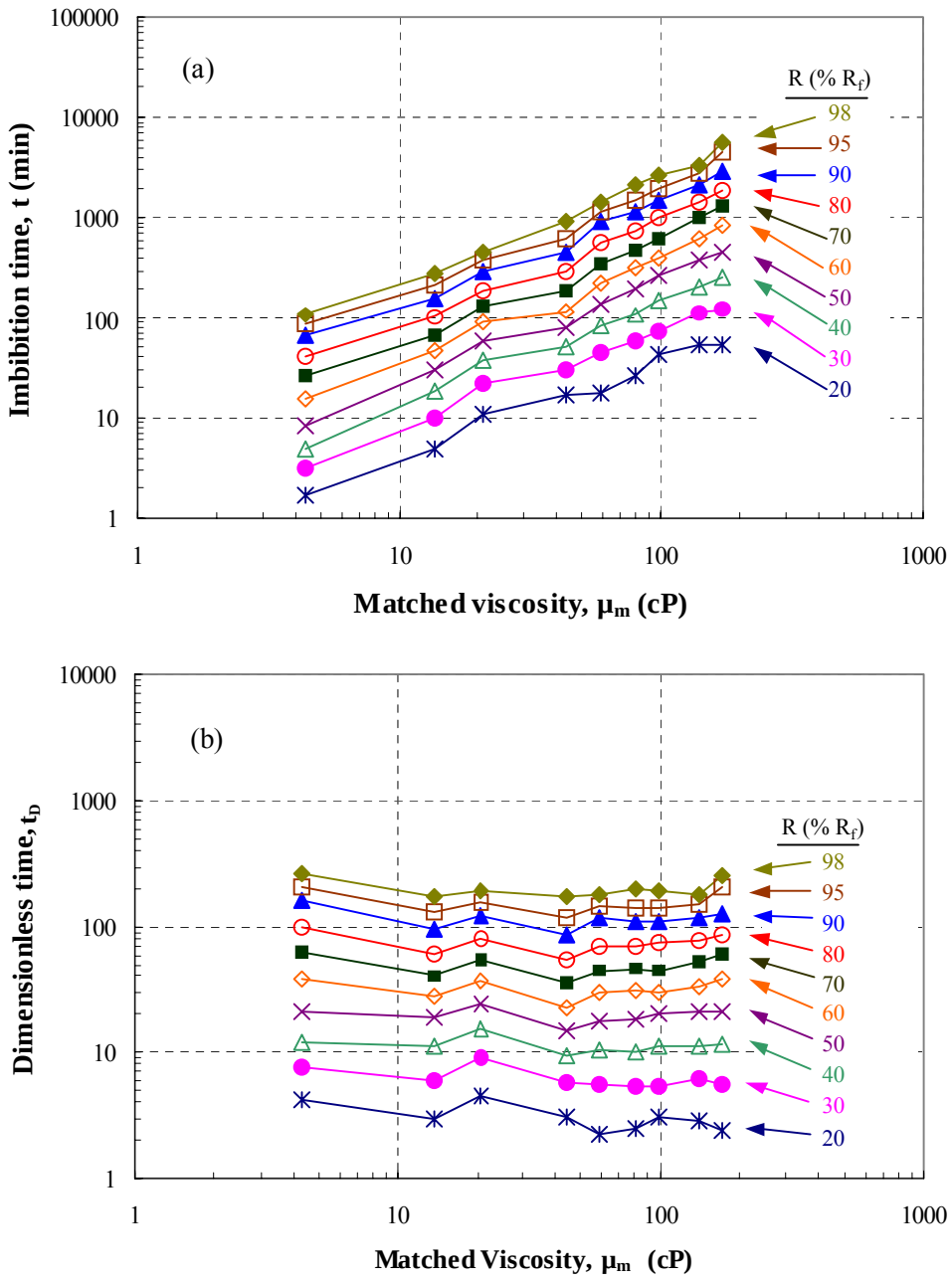

Fig. 4.2. Imbibition time (a) and scaled time (b) versus matched viscosity for fractional recoveries, R, ranging from 20 % to 98 % (interpolated values for individual cores).

Task 5. *Comparison with similarity solutions.*

Results and Discussion

The objective of Task 5 is to compare results given by simulation with special case analytic results given by similarity solutions for spontaneous imbibition for at least five distinct cases of rock and fluid properties. This task was completed with the verification presented in the last quarterly report (R05).

CONCLUSIONS

1. Petrophysical measurements on Berea sandstone used in spontaneous imbibition tests are reported. Surface areas measured by adsorption of nitrogen and water are in satisfactory agreement.
2. Mathematical network models are presented which provide a consistent account of dynamic phenomena associated with spontaneous imbibition. Observations on simple laboratory networks were confirmed by the behavior of a unit cell network model. For gas/oil increase in gas pressure is observed. The maximum pressure is marked by the start of gas production.
3. The basis for numerical simulation of imbibition is presented.
4. Satisfactory correlation of data for matched aqueous and oil phase viscosities were obtained for a viscosity range for 4 to 172cp.

REFERENCES

Barrett, E.P., Joyner, L.S. and, Halenda, P.P.; "The determination of pore volume and area distribution in porous substances I. Computations from nitrogen isotherms", J. Am. Chem. Soc. 73, 373-380 (1951)

Blair, P.M., "Calculation of Oil Displacement by Countercurrent Water Imbibition", *SPEJ*, Sept. 1964, 195-202.

Blunt, M.J.: "Pore Level Modeling of the Effects of Wettability," *SPEJ* (Dec. 1997) **2**, 494-510.

Churcher P.L., French P.R., Shaw J.C., Schramm L.L., "Rock properties of berea sandstone, baker dolomite, and indiana limestone", SPE International Symposium on Oilfield Chemistry held in Anaheim, California, February 20-22, 1991

Dixit, A.B., McDougall, S.R., Sorbie, K.S., and Buckley, J.S.: "Pore Scale Modelling of Wettability Effects and their Influence on Oil Recovery," *SPEREE* (Feb. 1999) **2**, 25-36.

Everett, D.H., “Manual of Symbols and Physicochemical Quantities and Units”, *J. Pure & Applied Chem.*, 31, 1972, 578-638.

Fischer, H., Morrow, N.R., Mason, G., “Application of water desorption/adsorption isotherms data to characterization of micro and mesoporosity in sandstone and carbonate rocks”, submitted for COPS 7, 7th International Symposium on Characterization of Porous Solids, Aix-en-Provence (France), May 26-28, 2005

Ma, S., Mason, G. and Morrow, N.R.: “Effect of Contact Angle on Drainage and Imbibition in Regular Polygonal Tubes,” PS-1191, *Colloids and Surfaces,* **117**, 1996, 273-291.

Mason, G., “A Model of the Pore Space in a Random Packing of Equal Spheres”, *J. Colloid Interface Sci.*, 35, 1971, 279-287.

Mason, G., Nguyen, M.D., and Morrow, N.R.: "Effect of Contact Angle on the Meniscus Between Two Equal Contacting Rods and a Plate," *J. Coll. Inter. Sci.,* 1983, **95**, 494.

Mason, G. and Morrow, N.R.: "Meniscus Displacement Curvatures of Perfectly Wetting Liquid in Capillary Pore Throats Formed by Spheres," *J. Coll. Inter. Sci.,* Jan. 1986, **109**, 46-56.

Mason, G. and Morrow, N.R.: "Meniscus Configurations and Curvatures in Non-Asymmetric Pores of Open and Closed Uniform Cross-Section," *Proc. Royal Soc.* London, 1987, **A414**, 111-33.

Mason, G. and Morrow, N.R.: "Capillary Behavior of a Perfectly Wetting Liquid In Irregular Triangular Tubes," *J. Coll. Inter. Sci.,* Jan. 1991, **141**, 262-74.

Oulton, T.D., “The pore size-surface area distribution of a cracking catalyst”, J. Phys. Chem. 1948 52(8) 1296-1314

Øren, P.-E., Bakke, S., and Arntzen, O.J.: “Extending Predictive Capabilities to Network Models,” *SPEJ* (Dec. 1998) 324-336.

Pooladi-Darvish, M. and Firoozabadi, A., “Experiments and modeling of water injection in water-wet fractured porous media”, *J. Can. Pet. Tech.,* March 2000, 39, 3:31-42.

Ruth, D., Morrow, N.R., Li, Y., Buckley, J.S., “A simulation study of spontaneous imbibition”, Proceedings of the International Symposium of the Society of the Core Analysts Annual Meeting, Oct. 2000, Abu Dhabi, UAE.

Richtmyer, R.D., and Morton, K.W., *Difference Methods for Initial-Value Problem*, 2nd edn., 1973, Interscience Publishers, New York.

Shull, C.G., “The determination of pore size distribution from gas adsorption data”, J. Am. Chem. Soc. 70, 1405, 1948.

Wheeler, A., “Presentations at catalysis symposia”, Gibson Island A.A.A.S. Conferences, June 1945 and June, 1946

Zhang, X., Morrow, N.R., and MA, S., “Experimental verification of a modified scaling group for spontaneous imbibition”, *SPE Reservoir Engineering*, Nov. 1996, pp.280-285.